Available online at www.sciencedirect.com
ScienceDirect
Earth and Planetary Science Letters 252 (2006) 152–161
EPSL
www.elsevier.com/locate/epsl

Al_2O_3 incorporation in $MgSiO_3$ perovskite and ilmenite

Wendy R. Panero [a,*], Sofia Akber-Knutson [b], Lars Stixrude [c]

[a] Department of Geological Sciences, Ohio State University, Columbus, OH 43210, United States
[b] Institute of Geophysics and Planetary Physics, University of California, San Diego, La Jolla, CA 92093-0225, United States
[c] Department of Geological Sciences, University of Michigan, Ann Arbor, MI 48109, United States

Received 17 May 2006; received in revised form 19 September 2006; accepted 21 September 2006
Available online 31 October 2006
Editor: S. King

Abstract

First-principles calculations in the $MgSiO_3$–Al_2O_3 system predict that $MgSiO_3$–perovskite dissolves about 15 mol% Al_2O_3 at the top of the lower mantle, limited by coexistence with Al-rich ilmenite (corundum). The solubility increases with pressure so that the lower mantle is likely undersaturated in alumina in all but the coldest parts of the uppermost lower mantle. The akimotoite–corundum solid solution is highly non-ideal with a symmetric regular solution parameter $W=66$ kJ/mol per formula unit at the top of the lower mantle. The critical temperature for exsolution of ilmenite is predicted to be 2000 K. The $MgSiO_3$ solution is also significantly non-ideal; assuming only Tschermak substitutions, the value of $W=12$ kJ/mol per formula unit. Total energy calculations over a range of compositions and several configurations for each composition are based on density functional theory in the local density approximation. We find that the entropy of solution of both structures is nearly ideal on the basis of random sampling of simulations using semi-empirical interatomic potentials. Results also confirm previous experimental and computational results showing that aluminum has little effect on the elasticity of $MgSiO_3$ perovskite.

Keywords: perovskite; first-principles calculations; mantle; alumina; solubility

The Earth's lower mantle (660–2900 km depth), accounting for about 60% of the Earth's volume, is dominated by the perovskite mineral phase. The Al_2O_3 content of the lower mantle is approximately 4% [1] and most of the aluminum appears to dissolve into the $MgSiO_3$ perovskite phase [2]. Many early experiments indicated that the solubility of alumina in perovskite was very limited and that a separate aluminum rich phase may exist in the lower mantle [3,4]. Determination of the solubility of Al_2O_3 in perovskite is hampered by difficulty in overcoming kinetic barriers in high-pressure experiments. Such experiments also have difficulty in detecting minor phases that might exsolve or not convert from initially amorphous or crystalline starting materials. Furthermore, these experiments cannot readily control the site into which the aluminum is substituted, possibly leading to discrepancies in the inferred density and equation of state of solid solutions [5].

Phase diagrams in the $MgSiO_3$–Al_2O_3 system, derived from solid solution calorimetry, are restricted to pressures below 30 GPa and indicate limited (~15 mol %) solubility of Al_2O_3 in perovskite at 26 GPa and 1873 K [6], limited by coexistence with an Al-rich

* Corresponding author.
E-mail address: panero.1@osu.edu (W.R. Panero).

0012-821X/$ - see front matter © 2006 Elsevier B.V. All rights reserved.
doi:10.1016/j.epsl.2006.09.036

ilmenite structured phase. Hirose et al. [7] find a solubility of 13 mol% Al_2O_3 at 25 GPa and 1750 °C (2023 K), consistent with calorimetry. Experiments at higher pressures on the pyrope ($Mg_3Al_2Si_3O_{12}$) composition show no secondary aluminum phase up to 84 GPa (2000–2500 K) [8], with complete transformation to *Pbnm* perovskite (25 mol% Al_2O_3) at 37 GPa and 1873 K [9].

Here we present the results of first-principles calculations aimed at determining the phase relations in the $MgSiO_3$–Al_2O_3 system throughout the pressure–temperature regime of the bulk of the lower mantle. In this regime, previous theory and experiment indicate that only two phases are stable on the join: perovskite and ilmenite. This two-phase coexistence is bounded at low pressure by the stabilization of garnet at about 26 GPa, and at high pressure by the transformation of corundum to the rhodium oxide phase near 80–100 GPa [10,11] and the transformation of perovskite to post-perovskite near 120 GPa [12]. The only other phases to have been proposed on this join are high-pressure polymorphs of spinel with calcium ferrite and calcium titanate structure [13,14], which would coexist with silica on the join of interest. However, density functional theory find that these phases are unstable with respect to decomposition into oxides on their own composition [15] and our own calculations confirm this result (unpublished results). On the join of interest, Brownmillerite-type substitution of Al in perovskite is expected to be negligible [16–20]; we consider only the Tschermak substitution.

1. Theory

The Gibbs free energy of a phase consisting of a binary solid solution of components A and B is

$$G(x,P,T) = x_A G_A(P,T) + x_B G_B(P,T) + TS_{sol}(x) + H_{sol}(x,P) \quad (1)$$

Where x_i and G_i are the mole fraction and Gibbs free energy, respectively, of end-member component i, T is temperature, and S_{sol} and H_{sol} are the entropy and enthalpy of solution, respectively, $x_A+x_B=1$, and x stands for $[x_A,x_B]$. In writing Eq. (1) the enthalpy of solution is assumed to be independent of temperature, and the entropy of solution is assumed to be independent of pressure and temperature, as it would be for ideal or regular solutions. These assumptions are consistent with experimental data on a number of mantle phases. Equilibrium coexistence with phase β consisting of a binary solid solution of the same components A and B is given by the equality of the chemical potentials of the two components in the coexisting phases. This can be written as

$$\left(\frac{dG^{\beta}_{sol}(x,P,T)}{dx_B}\right)_{x_B=x_B^{\beta}} - \left(\frac{dG^{\alpha}_{sol}(x,P,T)}{dx_B}\right)_{x_B=x_B^{\alpha}} = -\Delta G_B \quad (2)$$

where $G_{sol}=H_{sol}-TS_{sol}$ and $\Delta G_B=G_B^{\beta}-G_B^{\alpha}$ which, together with the similar equation for component A may be solved simultaneously for the equilibrium compositions of the two phases x_B^{α} and x_B^{β} if the difference in the end-member Gibbs free energies ΔG_B, ΔG_A, and the entropies and enthalpies of solution are known.

In our static (T=0 K) calculations, we compute the enthalpy of solution for several compositions of ilmenite and perovskite with Tschermak-type Al substitutions (Fig. 1) as the heats of reaction of

$$(1-x)MgSiO_3(pv) + xAl_2O_3(pv) = Mg_{1-x}Al_{2x}Si_{1-x}O_3(pv) \quad (3)$$

and

$$(1-x)MgSiO_3(ak) + xAl_2O_3(cor) = Mg_{1-x}Al_{2x}Si_{1-x}O_3(il) \quad (4)$$

where pv refers to the *Pbnm* perovskite structure, and ak and cor refer to the akimotoite (*R-3*) and corundum (*R-3c*) structures of the end member compositions, and il to the ilmenite-structured solid solution. We assume that the entropy of solution is ideal, an assumption that we test via additional computations as described below. The phase equilibrium determination is completed by assuming that the quantities ΔG_i are independent of temperature, and are therefore equal to corresponding differences in enthalpy among the end-member compositions on the left-hand side of Eqs. (3) and (4). This is justified by the observation that mantle phase transitions are primarily pressure- rather than temperature-driven [21] and that entropies of solid–solid reactions in the mantle are small fractions of the absolute entropy. We consider the effects of the temperature dependence of the ΔG_i further in the discussion.

We find, as described below, that the enthalpy of solution for Tschermak substitutions follows closely that of symmetric regular solutions, yielding for the Gibbs free energy of solution per formula unit

$$G_{sol}(x,P) = 2RT[x\ln x + (1-x)\ln(1-x)] + 2W(P)x(1-x) \quad (5)$$

where W is the regular solution parameter, and the ideal entropy of solution is computed assuming no Mg–Si

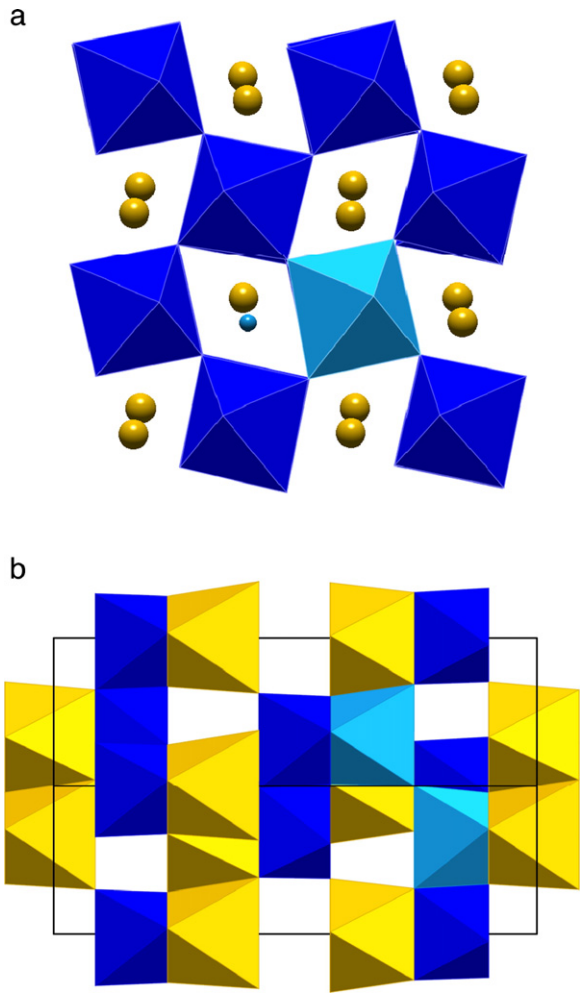

Fig. 1. The lowest energy structures for the Tschermak susbstitution in (a) perovskite (*Pbnm* as viewed on the (001) plane) and (b) ilmenite (*R-3* as viewed on the (110) plane). Dark blue is silicon, light blue aluminum and yellow is magnesium. The oxygen lattice is distorted very little by the Tschermak substitution: For oxygen neighboring an Al substitution, the maximum oxygen displacement is 0.12 Å (located between the Al_{Si}' and Al_{Mg}^{*}). Oxygen atoms in octahedra without a neighboring aluminum substitution aredistorted by no more than 0.04 Å.

disorder. The regular solution parameter is related to the critical temperature of exsolution by

$$T_C = \frac{W}{2R} \tag{6}$$

where R is the gas constant. The pressure dependence of W entails a non-linear dependence of the volume on composition

$$V(x) = x_A V_A + x_B V_B + x_A x_B V_{xs} \tag{7}$$

with $V_{xs}=2dW/dP$ the so-called excess volume, i.e. that part not accounted for in the ideal solution approximation.

1.1. Computations

Static, density functional theory calculations (VASP) were performed with the local-density approximation (LDA) and Vanderbilt-type ultrasoft pseudopotentials with a plane-wave expansion with a 600 eV energy cutoff [22–24]. The Brillouin zone is sampled with a $4\times4\times4$ mesh for those calculations with 36 or fewer atoms (e.g end member $MgSiO_3$ perovskite), and $2\times2\times2$ k-point sampling for larger calculations (up to 80 atoms, as was used for some intermediate compositions). Calculations of a single unit cell of end-member perovskite (20 atoms) with $4\times4\times4$ k-point sampling and a $2\times2\times1$ supercell (80 atoms) with $2\times2\times2$ k-point sampling result in atom positions that vary by no more than 0.01% in fractional atomic coordinates and total energies that differ by no more than 1 meV/atom. The *k*-point sampling and energy cutoff lead to values of the enthalpies of solution (Eqs. (3)–(4)) that are converged to be better than 0.1 meV.

All structures are fully relaxed. In the case of the solid solutions, this involves lowering of the symmetry, which is broken by the presence of defects. Solid solution calculations in the perovskite series were run for alumina fractions $x=1/16$, 1/4, 1/2, 3/4 and 15/16. Large supercells (80 atoms, $2\times2\times1$ *Pbnm* supercell) are required to capture the extremes of this series, while the other compositions were explored within the 20 atom *Pbnm* unit cell. Solid solution calculations in the akimotoite–corundum series were run for $x=1/6$, 1/3, 1/2, 2/3 and 5/6. For this series, we used the 30 atom hexagonal conventional cell. For each composition, we have investigated several different configurations.

In the case of ilmenite, we further investigate the configurational entropy by performing multiple simulations of random configurations following closely the methodology of previous work on aluminous perovskite [17].

1.2. Corrections to static calculations

Our calculations are static: they do not include the effects of lattice vibrations. In order to compare our predicted physical properties more directly with room temperature experimental observations, we estimated the effects of lattice vibrations from a simple model of the vibrational density of states. We consider the pressure due to zero-point motion, P_{zp} and the thermal pressure, P_{th} at 300 K [25].

The zero-point energy, E_{zp} is

$$E_{zp} = \sum_{i}^{3n} \frac{\hbar}{2}\omega_i = 3n\hbar\omega/2 \quad (8)$$

where $\hbar$ is Planck's constant divided by 2π, $3n$ is the number of modes per formula unit, ω_i is the vibrational frequency of each mode, and $\hbar$ is the mean frequency. The zero-point pressure is given by the volume derivative:

$$P_{zp} = -\left(\frac{\partial E_{zp}}{\partial V}\right)_T = -\frac{3n\hbar}{2}\frac{\partial \omega}{\partial V} \quad (9)$$

We adopt the Debye model of the vibrational density of states. The Debye temperature, Θ_D, is related to the mean vibrational frequency as

$$\frac{3}{4}k_B\Theta_D = \hbar\omega \quad (10)$$

where k_B is the Boltzmann's constant. Defining the Grüneisen parameter

$$\gamma = -\frac{\partial \ln\omega}{\partial \ln V} = -\frac{V}{\omega}\frac{\partial \omega}{\partial V} \quad (11)$$

the zero-point pressure is

$$P_{zp} = \frac{9n\gamma}{8}\frac{k_B\Theta_D}{V} \quad (12)$$

For perovskite, with Θ_D=888 K [26,27], γ=1.4 [28], and a volume per atom V/n=7.99 Å^3, the zero-point pressure correction is 2.4 GPa. For all ilmenite structures we assume Θ_D=912 K [26,27] and γ=1.5. For akimotoite, with V/n=8.62 Å^3 the zero-pressure, zero-point pressure correction is 2.5 GPa. The values of Θ_D and γ are assumed to be volume dependent (the logarithmic volume derivative of γ q=1) but otherwise independent of composition across each solid–solution series.

In the Debye approximation, the thermal energy is

$$E_{th} = 9nk_BT(T/\Theta_D)^3\int_0^{\Theta_D/T}\frac{x^3}{e^x-1}dx \quad (13)$$

and the thermal pressure is

$$P_{th} = -\left(\frac{\partial E_{th}}{\partial V}\right)_T = \frac{\gamma}{V}E_{th} \quad (14)$$

Assuming Θ_D and γ as above, we find that the zero-pressure, 300 K thermal pressure is 0.6 GPa for both perovskite and akimotoite. This results in a total pressure correction from static calculations to 300 K of 3.5 GPa for perovskite and 3.1 GPa for akimotoite.

2. Results

2.1. End member structures

A comparison of the relaxed zero-pressure lattice parameters, volumes, and bulk moduli (Fig. 2) to published experimental and theoretical results shows excellent agreement for $MgSiO_3$ perovskite (*Pbnm*), $MgSiO_3$-akimotoite (*R-3*), and Al_2O_3–corundum (*R-3c*) [8,10,16,17,29–32]. Zero-pressure volume results are generally within 1% of previous LDA first-principles results, and when corrected to 300 K results generally within published experimental uncertainties. Bulk modulus values are also within experimental uncertainties when compared to experimental results. The perovskite (*Pbnm*)-structured Al_2O_3 end-member is fictive. We find excellent agreement with regards to *b*/*a* and *c*/*a* ratio, unit cell volume and bulk modulus (differences <0.5%) when compared to previous complementary calculations [10].

2.2. Perovskite solid solutions

Addition of Al_2O_3 in mantle-relevant amounts has a small effect on the volume and bulk modulus. For x_{Al}=1/16, the volume is 0.3% greater and the bulk modulus is 1% smaller than for the $MgSiO_3$ end-member (Fig. 2c,d). The rate of change of the volume with aluminum content (5.1%/x_{Al}) agrees with the experimental value of 5.8±0.7%/x_{Al} [8], as does the rate of change of the bulk modulus: 16%/x_{Al} for our results versus 27±14%/x_{Al} experimentally [8]. The dependence of volume on x_{Al} for larger Al contents becomes slightly non-linear. Our results can be represented by (Eq. (7)) with V_{xs}=1.63 Å^3. The dependence of the unit cell shape on Al content agrees perfectly with experimental data for perovskite synthesized along the $MgSiO_3$–Al_2O_3 join (Fig. 2). The orthorhombic distortion increases with increasing Al content in agreement with the analysis of Walter et al. [8]. We can rationalize this result microscopically as we find that the Al octahedra are rotated more than the Si octahedra so that as their proportion increases the unit cell deviates more from cubic. For example, in the x_{Al}=1/16 case with nearest Al–Al distance, the octahedron is rotated an additional 2.6° as compared

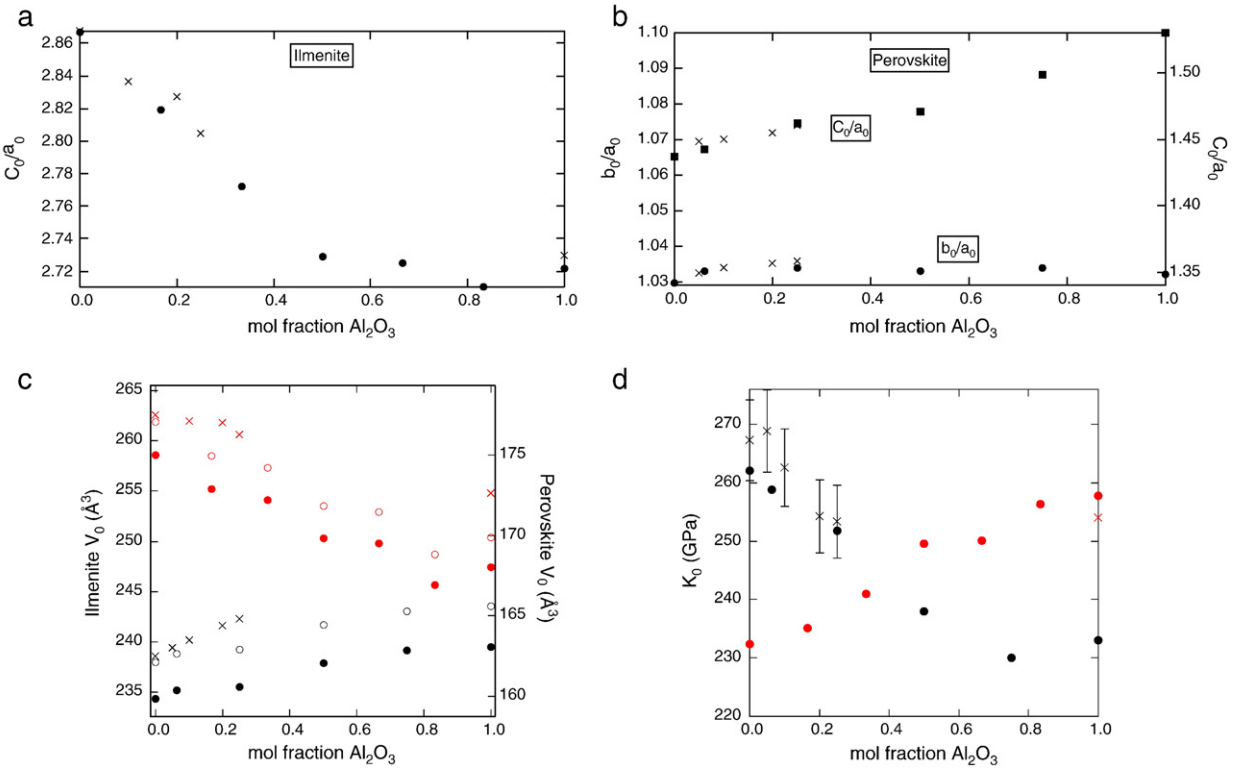

Fig. 2. (a) Ilmenite c_0/a_0 (b) Perovskite c_0/a_0 and b_0/a_0 (c) V_0 as a function of composition for perovskite (black) and ilmenite (red). Open symbols represent values corrected to 300 K. (d) K_0 as a function of composition for perovskite (black) and ilmenite (red). Crosses indicate experimental values from Walter et al. [8] (perovskite) and Akaogi et al. [34] (ilmenite).

with the Si octahedra (Fig. 1a), an amount that does not vary significantly with pressure.

For $x_{Al}=1/16$ (2 Al in an 80 atom unit cell), we examine two end-member configurations, one in which the Al atoms occupy neighboring dodecahedral and octahedral sites (Al–Al distance<3 Å), and another in which they are as distant as possible within the constraints of translational symmetry of the supercell (Al–Al distance=5.9 Å at 0 GPa). We find that the enthalpy of solution (Eq. (3)) differs by only 18 meV per formula unit or 15% for these two cases, implying that the solution is nearly ideal. These results agree with those of Yamamoto et al. [16] who investigated configurations with intermediate Al–Al distances as well, which led to intermediate values of the enthalpy of solution (Fig. 3). We find similarly small differences among different configurations for other values of the Al content. Our results therefore agree well with those of Akber-Knutson and Bukowinski [17] who find from their random sampling of configurations that the entropy of solution is 96% of the ideal value at 2000 K for perovskite with Tschermack substitutions.

2.3. Ilmenite solid solutions

Based on our results at $x_{Al}=0$, and $x_{Al}=1/6$, the addition of alumina to akimotoite decreases the volume

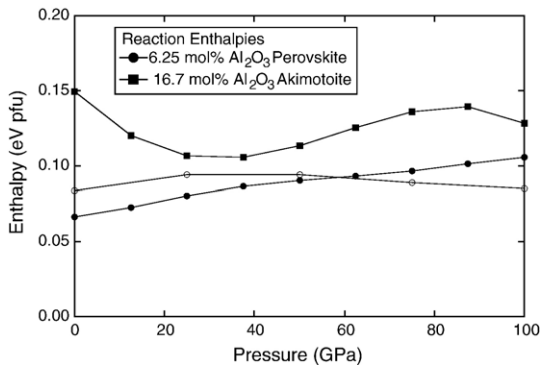

Fig. 3. Formation enthalpy per formula unit as a function of pressure for Al_2O_3 substitutions in the perovskite structure ($MgSiO_3$(pv)+Al_2O_3(cor)=(Mg,Al)(Si,Al)O_3). Solid symbols are the formation enthalpy based on calculations presented here (LDA), and open symbols show formation enthalpy results using GGA [16], where circles represent Tschermack substitutions in perovskite and squares represent substitutions in akimotoite.

initially at a rate of −7.9%/x_{Al}; this effect on akimotoite is significantly larger and of opposite sign to the effect on the volume of perovskite. This result is rationalized in terms of the cation radii: Al^{3+} is 25% larger than Si^{4+}, but 35% smaller than Mg^{2+} in octahedral coordination [33]. For larger Al contents the dependence of volume on compositions becomes non-linear. Our results may be represented by Eq. (7) with V_{xs}=7.2 Å^3. Previous experimental studies have not indicated a significantly non-zero value of V_{xs} [34], but the ability of these measurements to resolve the value of V_{xs} is limited by precision of the unit cell determination and the compositional range over which measurements on intermediate compositions have been made (x_{Al}=0–25%). The influence of Al content on the bulk modulus is very similar in magnitude to that in perovskite but of the opposite sign with corundum stiffer than akimotoite. The change in sign is related to the anisotropic distribution of Mg and Si in the ilmenite structure that makes the akimotoite end-member very anisotropic in compression as compared with corundum [32].

The effect of the substitution of Mg and Si into the corundum structure is to systematically increase the *c*/*a* ratio from 2.72 for corundum to 2.87 for akimotoite (Fig. 2a), in good agreement with experiment [34].

In contrast to the behavior of Al_2O_3 in perovskite, the total energy of ilmenite solid solutions is quite sensitive to the Al_{Mg}–Al_{Si} (or Mg_{Al}–Si_{Al}) distance and connectivity. In the case of x=1/6, the lowest energy substitution is through corner-linked octahedra with an Al–Al spacing of 3.4 Å. At 0 GPa, the energy difference between the lowest energy arrangement and the highest with a 7 Å Al–Al distance is 140 meV pfu, increasing to about 170 meV pfu at 50 GPa. It is therefore not immediately apparent, as it was in the case of perovksite, that the entropy of solution is ideal, nor how to represent the enthalpy of solution. In principle one would have to compute the partition function by computing the total energy of all possible defect arrangements for each composition, a computationally impossible task at present.

In order to further investigate the solution properties of ilmenite, we used a computationally faster scheme for sampling configuration space [17] based on a semi-empirical pair potential that permits calculation of the total energy in small fraction of the time required in density functional theory at the cost of accuracy. When comparing corner-linked and edge-linked substitutions at fixed volume, the difference between these substitutions is 67 meV per formula unit at 0 GPa for VASP and 65.5 meV per formula unit for the empirical calculations, resulting in a difference of just 2%. 2000 configurations of 16.7 mol% Al_2O_3 in akimotoite were randomly chosen in the 120-atom super-cell, using methods identical to those in [17] but with pair potentials modified from Matsui et al. [35], and allowing for charge-coupled substitutions of aluminum for Mg and Si atoms, but no Mg–Si disorder. The resulting density of states is highly asymmetric and strongly weighted toward a narrow range of energies near the ground state, and with a wide low-density tail to high energies (Fig. 4). There is a slight tendency for configurations with face-sharing Al octahedral to have higher energy. More than 90% of the configurations lie within 0.04 eV of the lowest energy configuration significantly less than 0.17 eV thermal energy at 2000 K (total range of 0.185 eV compared to 0.140 eV from the VASP calculates). The entropy computed from this distribution at 2000 K is 99.96% of the ideal value. This justifies our assumption of ideal configurational entropy of ilmenite at mantle temperatures. The atomistic simulations are also significant in that they show that we can take the lowest-energy configuration at each composition as representative of the enthalpy of solution. In detail, this approach yields a lower bound on the enthalpy of solution so that our estimated interaction parameters will also be lower bounds. The difference between the lower bound and the actual value based on Fig. 4 should be less than a few hundredths of electron volts or a few kJ/mol.

For both perovskite and ilmenite, the lowest-energy charge-coupled enthalpies of solution display a generally parabolic dependence on composition between 0 and 100 GPa (Fig. 5a). This indicates that the solution of Al_2O_3 in $MgSiO_3$ within a structurally consistent solid solution series is well approximated as a symmetric regular solution.

2.4. Interaction parameters

Perovskite and ilmenite solid solutions obey symmetric regular solution behavior to within 6% of the solution enthalpy with the exception of the 16.7% $MgSiO_3$ composition in ilmenite where the residuals are ~30%. Including this composition in the determination of a best fitting symmetric interaction parameter does not significantly affect the results. The interaction parameter W_{pv} from our results is 5.1 kJ/mol per site, or 10.2 kJ/mol per formula unit at 30 GPa. This agrees well with the estimate made by Akaogi and Ito [6] based on differences in zero pressure volume (W_{pv}=5.6 kJ/mol per site).

For akimotoite, we find a very large interaction parameter W_{il}=33 kJ/mol per site or 66 kJ/mol per formula unit at 30 GPa. This is in contrast to the value

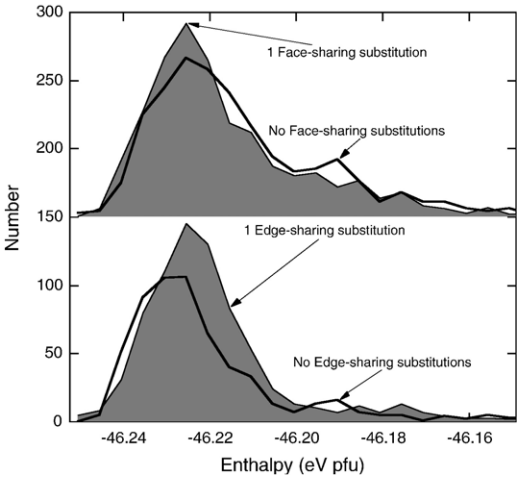

Fig. 4. Density of configurational states (enthalpy) for 2000 randomly chosen configurations in a 120-atom supercell of ilmenite with 16.7% Al_2O_3. (top) Black line shows the subset of those configurations with no face-sharing octahedra, while the grey fill shows those calculations with exactly one face-sharing octahedron. (bottom) Black line shows the subset of those configurations with no edge-sharing octahedra, while the grey fill shows those calculations with exactly one edge-sharing octahedron. Note that the thermal energy kT at 2000 K is 0.175 eV, about twice the horizontal scale of this figure.

predicted by the difference in experimental zero-pressure volumes of the end-members (2.6 kJ/mol), and to the inferred zero value determined by calorimetry [34] (ideal enthalpy of solution) within experimental errors.

The discrepancy with the estimate based on volume systematics likely arises from the limited applicability of the relationship between differences in the zero-pressure volume of end member compositions to the interaction parameter. Published correlations [36] only treat binary systems with one divalent substituting ion in a single, octahedral site. For multi-valent substitutions such as ilmenite, the influence of the two types of substitutions on the energy is large via local lattice distortion but small on the unit-cell volume as the substitutions tend to compensate each other. The apparent discrepancy with experimental data is more difficult to understand even within the substantial experimental uncertainties. One possibility is that the experimental samples have suffered exsolution, which would limit the measured enthalpy of solution to that of the spinodal composition and systematically produce values lower than our theoretical prediction. Indeed, our results predict that at the conditions of synthesis (1000 °C) spinodal exsolution occurs at $x_{Al}=0.25$, whereas equilibrium exsolution occurs at $x_{Al}=0.06$. The possibility of exsolution in ilmenite would require a re-interpretation of the low temperature phase diagram on the enstatite–pyrope join.

2.5. Phase equilibria

We calculate the phase diagram for the $MgSiO_3$–Al_2O_3 system between 20 GPa and 100 GPa at 2000 K and 3000 K assuming 100% configurational entropy (Fig. 6). At all temperatures and pressures over 20 GPa, we find increasing solubility with pressure of Al_2O_3 in $MgSiO_3$ perovskite. Likewise, increasing pressure decreases the solubility of $MgSiO_3$ in Al_2O_3–corundum. Along the $MgSiO_3$–Al_2O_3 join, alumina solubilities in perovskite increase from 15 mol% Al_2O_3 at 25 GPa to 31 mol% at 100 GPa at 2000 K and increase with increasing temperature. Experiments at the low pressure limit of the perovskite + corundum stability field are in good agreement with our results although there is some scatter in the experimental data: alumina solubility in perovskite is 10–14% at temperatures of 1873–2173 K

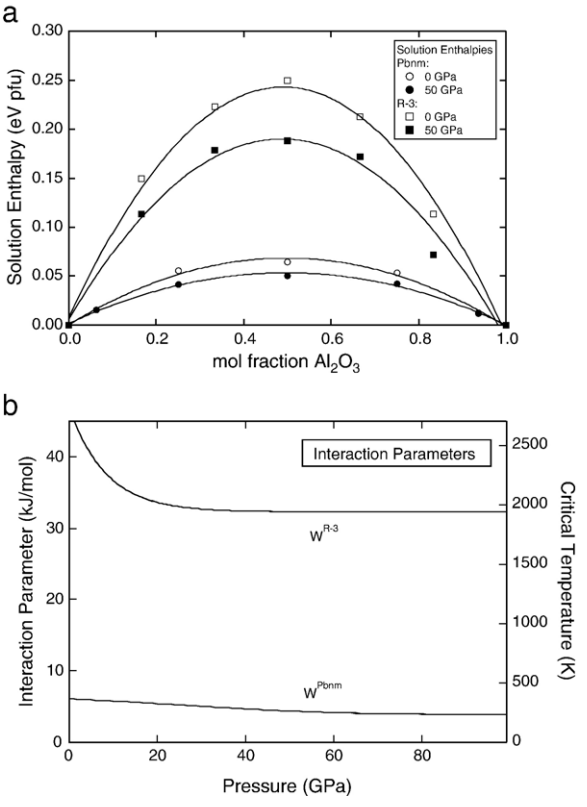

Fig. 5. (a) Excess enthalpy of solution of Al_2O_3 in perovskite (circles) and akimotoite (squares) at 0 GPa (open symbols) and 50 GPa (closed symbols). Curves represent the bet-fit regular solution model for each set. (b) Non-ideality interaction parameter, W, as a function of pressure for the two structures.

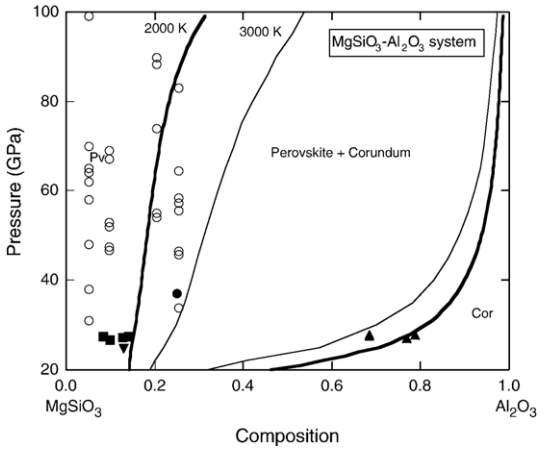

Fig. 6. Predicted phase boundaries at 2000 K (thick lines) and 3000 K (thin lines) compared with experimental measurements of compositions of coexisting perovskite (filled squares 1673–2173 K [37]; filled circle 1873 K [9]; inverted triangle 2023 K [7]) and ilmenite (filled triangle 1673–2173 K [37]); and the bulk compositions in which only perovskite was observed (open circles 2000–2600 K [8]).

[7,37] with a tendency for the solubility to increase with increasing temperature. Synthesis experiments with the pyrope ($Mg_3Al_2Si_3O_{12}$ x_{Al}=25%) composition show only a perovskite phase at 37 GPa [9], implying a more rapid increase in solubility with increasing pressure than we predict. The origin of this discrepancy is unclear. The dependence of the solubility on pressure is primarily a function of the partial molar volume of the alumina component in perovskite, which appears to be predicted correctly by our calculations (Fig. 2c).

Calculated solubilities of $MgSiO_3$ in corundum agree well with available experimental data. We find 22% solubility at 27 GPa and 2000 K decreasing with increasing pressure and increasing with increasing temperature as compared experimental data of 23 at 1872 K and 31% at 2173 K [37].

The phase diagram (Fig. 6) is constructed only with consideration of configurational entropy as discussed in the theory section. We may evaluate the influence of vibrational entropy on our calculations by considering the ilmenite to perovskite transition with an entropy change in the $MgSiO_3$ end-member of ΔS=5–13 J/mol/K [38,39] due to the effects of additional vibrational degrees of freedom in the perovskite structure. If we assume the same vibrational entropy contrast for the aluminous end-members, vibrational entropy tends to stabilize perovskite at the expense of ilmenite with increasing temperature. However, the effect on the solubility is small, increasing the solubility of Al_2O_3 in $MgSiO_3$ perovskite by 0.12%–0.4% and 0.3–0.7% at 25 GPa for 2000 K and 3000 K, respectively.

2.6. Conclusions

We calculate the phase diagram on the $MgSiO_3$–Al_2O_3 join at lower mantle pressure and show that perosvkite can dissolve significant amounts of Al_2O_3 under lower mantle conditions. The effects of aluminum on the volume and bulk modulus are minimal for the Tschermak substitution at likely mantle alumina contents. Experimental results showing a larger effect of Al on the bulk modulus may be based on samples in which Al is incorporated via a different substitution mechanism, such as the Brownmillerite mechanism, that is thought to be much less important throughout most of the lower mantle.

The configurational entropy in the $MgSiO_3$–Al_2O_3 is likely ideal for both the perovskite (*Pbnm*) and ilmenite (*R-3*) structures. Both solutions have substantial enthalpies of solution, and ilmenite has an exceptionally large interaction parameter of 33 kJ/mol per site, larger than that of diopside, for example.

The $MgSiO_3$–Al_2O_3 join may be considered a basis from which to understand lower mantle phase equilibria in more complex compositions. While the solubility of alumina in perovskite is greater than the alumina content of pyrolite, it is less than that of basalt. Basalt is therefore likely to have other aluminous phases in addition to perovskite. Indeed experiments show a calcium ferrite phase in basalt compositions [14]. This phase is likely stabilized also by the presence of large amounts of calcium in basalt since density functional calculations indicate that end-member $MgAl_2O_4$ is unstable [15] and that experimental observations of calcium ferrite of spinel composition [13,14] may be influenced by reaction kinetics. The lower mantle has excess MgO as compared with the join of our study. This may stabilize the brownmillerite form of Al substitution into perovskite and alter the Al solubility [5,20] at least in the upper part of the lower mantle where this vacancy assisted mechanism is thought to be most important [17]. $MgSiO_3$–perovskite and MgO in the mantle will in fact contain about 10 mol% FeO. The effect of these solid solutions will be to lower the effective activity of each component and raise the configurational entropy. Aluminum apparently interacts differently with ferrous and ferric iron in perovskite [40]. Indeed, Nishi-Hamane et al. [41] find that $MgSiO_3$–perovskite dissolves 15 mol% Al_2O_3 between 24 and 51 GPa in the $MgSiO_3$–$FeAlO_3$ system. This reaction may be energetically favorable and thereby suggest that a mantle dominated by ferric iron greatly enhances the solubility of aluminum in perovskite. The possibility of additional charge-couple substitutions involving aluminum, such as $H^+Al^{3+}=Si^{4+}$, further enrich the picture [42].

Acknowledgements

Calculations were performed on the Ohio Supercomputer Center with award #PAS0238-1, and additional support for this work comes from NSF #EAR-0537813.

References

[1] W.F. McDonough, S.-S. Sun, The composition of the Earth, Chem. Geol. 120 (1995) 223–253.
[2] T. Irifune, Absence of an aluminous phase in the upper part of the Earth's lower mantle, Nature 370 (1994) 131–133.
[3] E. Ito, E. Takahashi, Ultrahigh pressure phase transformations and the constitution of the deep mantle, in: M.H. Manghnani, Y. Syono (Eds.), High-Pressure Research in Mineral Physics, Terra Pub, Tokyo, 1989, pp. 221–229.
[4] B. O'Neill, R. Jeanloz, $MgSiO_3$–$FeSiO_3$–Al_2O_3 in the Earth's lower mantle: perovskite and garnet at 1200 km depth, J. Geophys. Res. 99 (1994) 19901–19915.
[5] A. Navrotsky, M. Schoenitz, H. Kojitani, H. Xu, J. Zhang, D.J. Weidner, R. Jeanloz, Aluminum in magnesium silicate perovskite: formation, structure, and energetics of magnesium-rich defect solid solutions, J. Geophys. Res. 108 (2003), doi:10.1029/2002JB002055.
[6] M. Akaogi, E. Ito, Calorimetric study on majorite–perovskite transition in the system $Mg_4Si_4O_{12}$–$Mg_3Al_2Si_3O_{12}$: transition boundaries with positive pressure–temperature slopes, Phys. Earth Planet. Inter. 114 (1999) 129–140.
[7] K. Hirose, Y. Fei, S. Ono, T. Yagi, K. Funakoshi, Measurements of the phase transition boundary in $Mg_3Al_2Si_3O_{12}$: implications for the nature of the seismic discontinuities in the Earth's mantle, Earth Planet. Sci. Lett. 184 (2001) 567–573.
[8] M.J. Walter, A. Kubo, T. Yoshino, J.P. Brodholt, K.T. Koga, Y. Ohishi, Phase relations and equation-of-state of aluminous Mg-silicate perovskite and implications for Earth's lower mantle, Earth Planet. Sci. Lett. 222 (2004) 501–516.
[9] E. Ito, A. Kubo, T. Katsura, M. Akaogi, T. Fujita, High pressure transformation of pyrope ($Mg_3Al_2Si_3O_{12}$) in a sintered diamond cubic anvil assembly, Geophys. Res. Lett. 25 (1998) 821–824.
[10] K.T. Thomson, R.M. Wentzcovitch, M.S.T. Bukowinski, Polymorphs of alumina predicted by first principles: putting pressure on the ruby pressure scale, Science 274 (1996) 1880–1882.
[11] N. Funamori, R. Jeanloz, High-pressure transformation of Al_2O_3, Science 278 (1990) 1109–1111.
[12] M. Murakami, K. Hirose, K. Kawamura, N. Sata, Y. Ohishim, Post-perovskite phase transition in $MgSiO_3$, Science 304 (2004) 855–858.
[13] W.R. Panero, L.R. Benedetti, R. Jeanloz, Transport of water into the lower mantle: role of stishovite, J. Geophys. Res. 108 (2003), doi:10.1029/2002JB002053.
[14] K. Hirose, F. Yingwei, Y. Ma, H.K. Mao, The fate of subducted basaltic crust in the Earth's lower mantle, Nature 397 (1999) 53–56.
[15] L. Gracia, A. Beltran, J. Andres, R. Franco, J.M. Recio, Quantum-mechanical simulation of $MgAl_2O_4$ under high pressure, Phys. Rev., B 66 (2002) 224114.
[16] T. Yamamoto, D.A. Yuen, T. Ebisuzaki, Substitution mechanism of Al ions in $MgSiO_3$ perovskite under high pressure conditions from first-principles calculations, Earth Planet. Sci. Lett. 206 (2003) 617–625.
[17] S. Akber-Knutson, M.S.T. Bukowinski, The energetics of aluminum solubility into $MgSiO_3$ perovskite at lower mantle conditions, Earth Planet. Sci. Lett. 220 (2004) 317–330.
[18] J.P. Brodholt, Pressure-induced changes in the compression mechanism of aluminous perovskite in the Earth's mantle, Nature 407 (2000) 620–622.
[19] J.F. Stebbins, S. Kroeker, D. Andrault, The mechanism of solution of aluminum oxide in $MgSiO_3$ perovskite, Geophys. Res. Lett. 28 (2001) 615–618.
[20] J.F. Stebbins, H. Kojitani, M. Akaogi, A. Navrotsky, Aluminum substitution in $MgSiO_3$ perovskite: investigation of multiple mechanisms by ^{27}Al NMR, Am. Mineral. 88 (2003) 1161–1164.
[21] R. Jeanloz, Thermodynamics of phase transitions, Rev. Mineral. 14 (1985) 389–428.
[22] G. Kresse, J. Furthmüller, Efficiency of ab-initio total energy calculations for metals and semiconductors, Comput. Mater. Sci. 6 (1996) 15–50.
[23] G. Kresse, J. Furthmüller, Efficient iterative schemes for ab initio total-energy calculations using a plane-wave basis set, Phys. Rev., B 54 (1996) 11,169–111,186.
[24] G. Kresse, D. Joubert, From ultrasoft pseudopotentials to the augmented-wave method, Phys. Rev., B, Condens. Matter 59 (1999) 1758–1775.
[25] J. Aidun, M.S.T. Bukowinski, M. Ross, Equation of state and metallization of CsI, Phys. Rev., B 29 (1984) 2611–2621.
[26] L. Stixrude, C. Lithgow-Bertelloni, Thermodynamics of mantle minerals-I. Physical properties, Geophys. J. Int. 162 (2005) 610–632.
[27] L. Stixrude, C. Lithgow-Bertelloni, unpublished.
[28] M. Akaogi, E. Ito, Heat capacity of $MgSiO_3$ perovskite, Geophys. Res. Lett. 20 (1993) 105–108.
[29] H. Horiuchi, M. Hirano, E. Ito, Y. Matsui, $MgSiO_3$ (Ilmenite-type) single-crystal X-ray diffraction study, Am. Mineral. 67 (1982) 788–793.
[30] B.B. Karki, W. Duan, C.R.S. da Silva, R.M. Wentzcovitch, Ab initio structure of $MgSiO_3$ ilmenite at high pressure, Am. Mineral. 85 (2) (2000) 317–320.
[31] Y. Wang, T. Uchida, J.Z. Zhang, M.L. Rivers, S.R. Sutton, Thermal equation of state of akimotoite $MgSiO_3$ and effects of the akimotoite–garnet transformation on seismic structure near the 660 km discontinuity, Phys. Earth Planet. Inter. 143 (2004) 57–80.
[32] L.W. Finger, R.M. Hazen, Crystal structure and compression of ruby to 46 kbar, J. Appl. Phys. 49 (1978) 5823–5826.
[33] R.D. Shannon, C.T. Prewitt, Effective inoic radii in oxides and fluorides, Acta Crystallogr. B25 (1969) 925–946.
[34] M. Akaogi, M. Tanaka, E. Ito, Garnet–ilmenite–perovskite transitions in the system $Mg_4Si_4O_{12}$–$Mg_3Al_2Si_3O_{12}$ at high pressures and high temperatures: phase equilibria, calorimetry and implications for mantle structure, Phys. Earth Planet. Inter. 132 (2002) 303–324.
[35] M. Matsui, G.D. Price, A. Patel, Comparison between the lattice-dynamics and molecular-dynamics methods — calculation results for $MgSiO_3$ perovskite, Geophys. Res. Lett. 21 (1994) 1659–1662.
[36] P.K. Davies, A. Navrotsky, Quantitative correlations of deviations from ideality in binary and pseudobindary solid solutions, J. Solid State Chem. 46 (1983) 1–22.
[37] A. Kubo, M. Akaogi, Post-garnet transitions in the system $Mg_4Si_4O_{12}$–$Mg_3Al_2Si_3O_{12}$ up to 28 GPa: phase relations of garnet, ilmenite and perovskite, Phys. Earth Planet. Inter. 121 (2000) 85–102.

[38] Akaogi Ito, Navrotsky Topor, Negative pressure–temperature slopes for reactions forming $MgSiO_3$ perovskite from calorimetry, Science 249 (1990) 1275–1278.
[39] R.M. Wentzcovitch, L. Stixrude, B.B. Karki, B. Kiefer, Akimotoite to perovskite phase transition in $MgSiO_3$, Geophys. Res. Lett. 31 (2004), doi:10.1029/2004GL019704.
[40] D.J. Frost, F. Langenhorst, The effect of Al_2O_3 on Fe–Mg partitioning between magnesiowüstite and magnesium silicate perovskite, Earth Planet. Sci. Lett. 199 (2002) 227–241.
[41] D. Nishi-Hamane, T. Nagai, K. Fujino, Y. Seto, Fe^{3+} and Al solubilities in $MgSiO_3$ perovskite: implications of $Fe^{3+}AlO_3$ substitution in $MgSiO_3$ perovskite at the lower mantle condition, Geophys. Res. Lett. 32 (2005) L16306, doi:10.1029/2005GL023529.
[42] W.R. Panero, L. Stixrude, Hydrogen incorporation in stishovite and symmetric hydrogen bonding in δ-AlOOH, Earth Planet. Sci. Lett. 221 (2004) 421–431.